Biophysical Journal Volume 100 March 2011 1446–1454

3_{10}-Helix Conformation Facilitates the Transition of a Voltage Sensor S4 Segment toward the Down State

Christine S. Schwaiger, Pär Bjelkmar, Berk Hess, and Erik Lindahl*
Theoretical and Computational Biophysics, Department of Theoretical Physics and Swedish e-Science Research Center, Royal Institute of Technology, Stockholm, Sweden

ABSTRACT The activation of voltage-gated ion channels is controlled by the S4 helix, with arginines every third residue. The x-ray structures are believed to reflect an open-inactivated state, and models propose combinations of translation, rotation, and tilt to reach the resting state. Recently, experiments and simulations have independently observed occurrence of 3_{10}-helix in S4. This suggests S4 might make a transition from α- to 3_{10}-helix in the gating process. Here, we show 3_{10}-helix structure between Q1 and R3 in the S4 segment of a voltage sensor appears to facilitate the early stage of the motion toward a down state. We use multiple microsecond-steered molecular simulations to calculate the work required for translating S4 both as α-helix and transformed to 3_{10}-helix. The barrier appears to be caused by salt-bridge reformation simultaneous to R4 passing the F233 hydrophobic lock, and it is almost a factor-two lower with 3_{10}-helix. The latter facilitates translation because R2/R3 line up to face E183/E226, which reduces the requirement to rotate S4. This is also reflected in a lower root mean-square deviation distortion of the rest of the voltage sensor. This supports the 3_{10} hypothesis, and could explain some of the differences between the open-inactivated- versus activated-states.

INTRODUCTION

Voltage-gated ion channels open in response to changes in the voltage across the membrane, and control neuronal excitations such as nerve signals and heart beats (1). All voltage-gated ion channels are comprised of four subunits each with six transmembrane helices (S1–S6). The first four form a voltage-sensing domain (VSD) with the positively charged S4 helix functioning as the voltage sensor, whereas S5 and S6 from all four subunits jointly form the pore domain, i.e., the ion permeation pathway.

The nature of the gating motion is vividly debated. The positively charged residues in S4 have been shown to be critical, and the N-terminal ones carry most of the gating current (2,3). This is due to movement of these residues in response to changes in the membrane electric field. The movement is propagated to the pore, leading to a conformational change that opens or closes it. The first experimental proof for this was gained from cysteine scanning by Horn (4), and evidence of actual distance changes were first observed with spectroscopy by Cha et al. (5) and Glauner et al. (6).

VSDs have been found to occur in isolation, as voltage-sensor-only proteins without the pore (7–9). Although some of these are believed to form dimers, they have been confirmed to function even as monomers (10), which provides for a nice model system.

The VSD is shaped like an hourglass with two aqueous crevices separated by a central hydrophobic constriction (11,12) that has been suggested to act as an energy barrier for gating (13). It has been proposed that the charged residues move along this partially aqueous pathway (14) and interact favorably with negatively charged residues in the S1–S3 segments. These residues are located in two clusters on each side of the central hydrophobic region, with two glutamates (E183 and E226 with Kv1.2/2.1 numbering) on the extracellular side, and a glutamate (E236) and aspartate (D259) on the intracellular side.

Although the details of gating are not yet fully understood, several models with different amount/ways of S4 rotation and translation have been proposed based on experimental data (compare, for instance, the transporter (15), helical screw (16–18), and paddle models (19)).

The variation of the gating models is largely due to the lack of crystal structures of the resting and intermediate states that would show conformations of the voltage-sensor along the gating pathway, but recent theoretical closed-state models of the Kv channel (20–22) have partly started to bridge the discrepancies.

The idea of S4 potentially adopting 3_{10}-helix structure is almost as old as the cloning of the first sodium channel (23), and was first put forward by Kosower (24). Although the first Kv1.2 structures had S4 in α-helical conformation, the recent Kv1.2/2.1 chimera structure (13) shows the intracellular end downstream of the third arginine (R3) forming a 10-residue 3_{10}-helix stretch (Fig. 1 *A*) (13). This revived the old idea, in particular when Clayton et al. (25) found an 11-residue 3_{10}-helix stretch in the MlotiK channel, and Shafrir et al. (26) proposed models for open/closed NaChBac that involved secondary structure changes.

The 3_{10}-helix hypothesis is supported by experiments of Villalba-Galea et al. (27) that identified three separate states: the resting (R) state would correspond to a closed channel; the active (A) state would correspond to the normally open

Submitted August 23, 2010, and accepted for publication February 2, 2011.
*Correspondence: erik@kth.se
Editor: Benoit Roux.

0006-3495/11/03/1446/9 $2.00
doi: 10.1016/j.bpj.2011.02.003

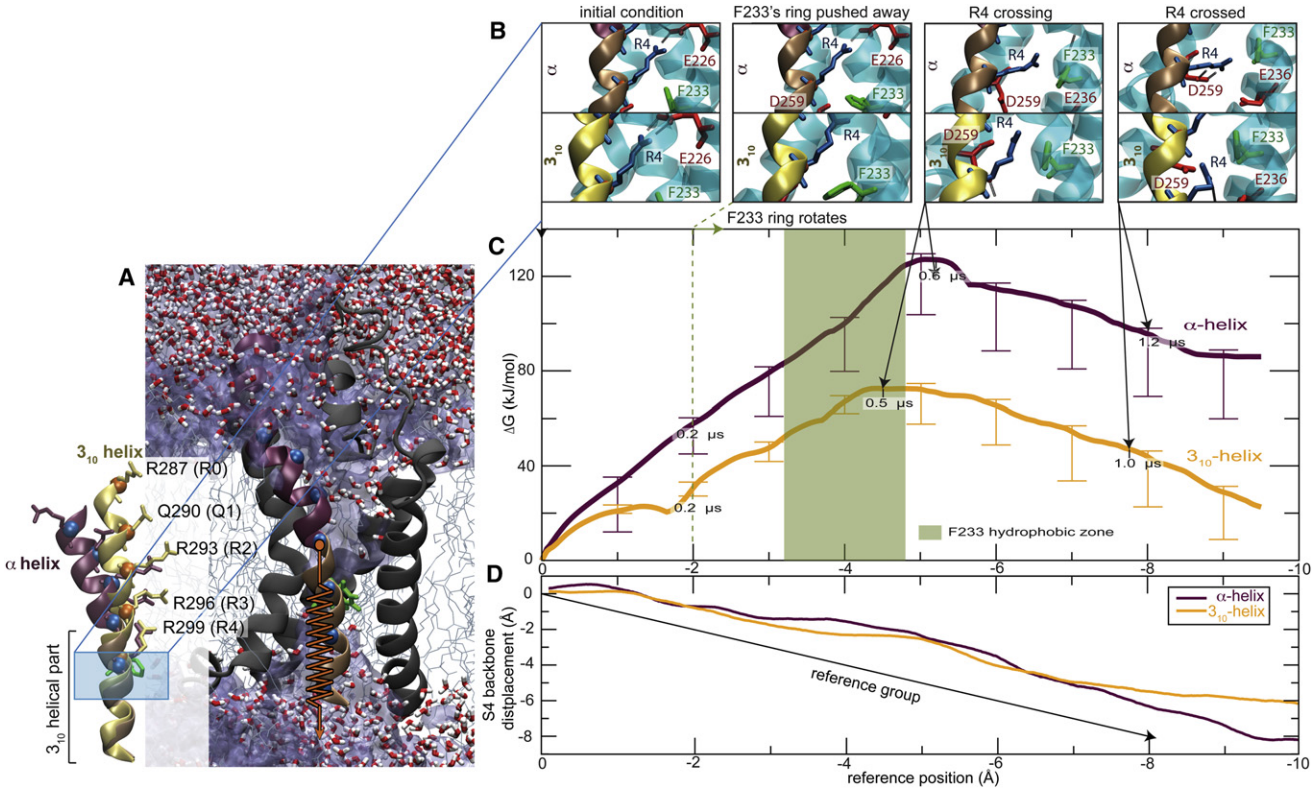

FIGURE 1 S4 down motion, as 3_{10}-helix requires less work than an α-helix. (*A*) VSD system and superimposed initial conformations of the α- and 3_{10} helices (*inset*). The upper α-helical part of the x-ray S4 structure is drawn dark, while its lower 3_{10} part is light. The 3_{10}-only helix is yellow. Charged residues (R0–R4) are marked with a sphere for C_α, with stick representation side chain and F233 is highlighted. (*B*) Characteristic events for a single side chain passing the hydrophobic zone close to F233 with S4 as α- and 3_{10}-helix, respectively. (*C*) Required work as a function of the pull reference displacement. It is almost a factor-two more advantageous for S4 to make the transition as an all-3_{10}-helix (~70 kJ/mol instead of ~130 kJ/mol), although this does not account for the potential α- to 3_{10}-helix conversion cost (see Discussion). Each work curve is a Jarzynski weighting (see Methods) from three separate 1–1.3 μs simulation trajectories with different random initial velocities. Standard errors are applied asymmetrically as this is an upper-limit estimate due to friction and noise effects. (*D*) S4 backbone displacement as a function of the pull reference displacement.

channel; and the relaxed (AL) state is an open-inactivated channel reached after prolonged depolarization (and possibly the one present in x-ray structures). Based on these experiments, including histidine scans, the S4 segment would normally adopt 3_{10}-helix conformation in the R and A states, but make a slow transition to α-helix in the AL state. In parallel, and independent from the experiments, several molecular simulations studies—started from older x-ray structures available before the chimera Kv1.2/2.1 structure—have observed the occurrence of 3_{10}-helix in the C-terminal part of S4 (22,28,29).

An important consequence of higher 3_{10}-helix contents is that S4 becomes tighter wound with three residues per turn, with aligned side chains pointing toward the VSD interior (27,28) (Fig. 2). This is critical, because the glutamate/aspartate residues in S2/S3 can stabilize the arginines during gating (18,30,31). With a predominant α-helix conformation in the upper part, the S4 segment would need to rotate (and potentially tilt) so the staircase-oriented staggered arginine side chains can maintain their strong interactions with the S2/S3 residues. Alternatively, if S4 initially (or progressively during gating) makes the transition to 3_{10}-helix, the segment will become slightly elongated and more tightly wound (Fig. 2 *B*). As a consequence, it will have slightly more space to move and the arginine side chains align on the same side of the helix, which would enable S4 to translate almost straight down while still maintaining its S2/S3 interactions, and likely cause much less distortion of the rest of the VSD (Fig. 2).

Interestingly, even early histidine scans pointed to 120° repeats that would be well fulfilled by a 3_{10}-helix, but alternative explanations were sought as S4 was then assumed to be in α-helical conformation (15). Thus, there are several indications of 3_{10}-helix in S4, if it was not for the important point that most of the segment is observed to be α-helical in the x-ray structure. In contrast to α-helices, the 3_{10}-helix is rare in crystal structures and mostly found in small regions of proteins, usually at the termini of an α-helix or as a separate single-turn helix (32). In membrane proteins, the transmembrane helices are virtually always α-helical. One reason for the low amount of 3_{10} is that the conformation is energetically unstable, essentially a kinetic intermediate

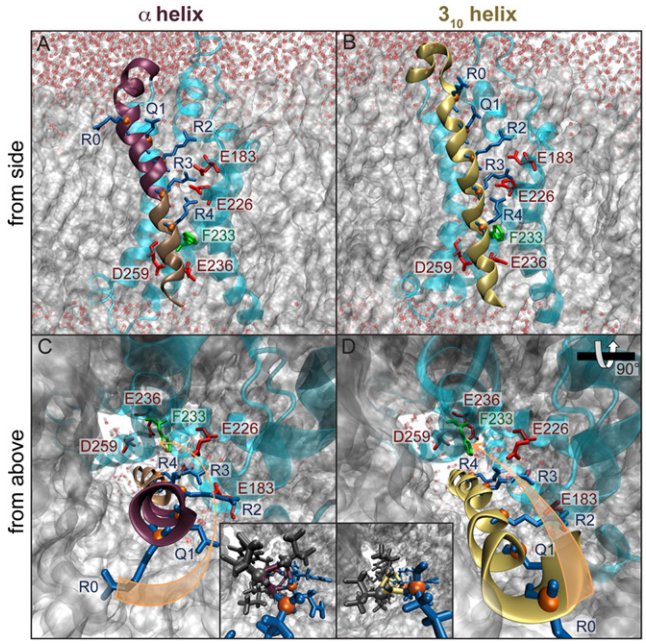

FIGURE 2 3_{10}-helix geometry facilitates S4 translation. (*A* and *B*) The arginine residues in the all-3_{10}-helix align perfectly, while they are rotated 60° around the helical axis relative to each other in the α-conformation. The α-helix will require major rotation and side-chain rearrangement for every arginine that passes the hydrophobic zone (*C*), while the 3_{10}-helix merely has to perform a minor initial rotation, after which it is able to translate almost straight down (*D*). The 120° turns in the 3_{10}-helix also place all side chains in a close to triangular shape, which together with a smaller radius should facilitate downward translation compared to the α-helix (*insets*).

along the α-helix unfolding pathway (33). However, for VSDs, it has been suggested that the 3_{10}-helix could be stabilized by the electric field (34), in addition to side-chain interactions. This seems to be supported by previous simulations (28) where 3_{10} growth in the open state was only observed with polarization applied.

Although it is difficult or impossible to completely model the gating process, we now address the more specific question of whether the 3_{10} secondary structure is responsible for facilitating the motion toward the down-state, or is merely present as a secondary effect. This would help us understand the voltage sensor movement, and potentially provide valuable insight about the character of the transition barrier.

Because there are no conformations available along the gating pathway, molecular simulation techniques are an obvious alternative to investigate the role of 3_{10} versus α-helix in S4. We use an isolated VSD as a model system, but even for small systems it is not possible to reach the multimillisecond timescales required for equilibrium transitions. Here, we have instead performed long nonequilibrium steered molecular simulations (SMD). Even this is not sufficient to cover the entire transition with statistical accuracy, but the process of consecutive side chains passing the hydrophobic zone appears to be similar. For this reason, we decided to focus on the part where the first S4 arginine (R4) crosses the hydrophobic zone, which makes it possible to do it slowly enough that the process is not dominated by friction, and obtain realistic intermediate conformations as well as quantitative work curves at least for the initial part of the process.

We have used both the x-ray structure for S4 (which we simply call "α-helix" despite the mixed structure), and an alternative conformation where we have forced an initial transition to all-3_{10}-helix, although the significant part is realistically limited to the region between Q1 and R3.

Both conformations were subject to multiple microsecond-scale simulations to obtain several independent trajectories from the initial position toward a more downward state. Some caution is advised when interpreting these results; the model only covers the initial gating, differences in secondary structure are extreme, and we are testing interactions rather than following a natural process. A steered simulation cannot exactly reproduce the influence of the electric field (35,36), and the simulations are short compared to the in vivo process. However, the model is very useful to study the specific interaction/work questions, including the potential causes of the barriers.

METHODS

System setup

The system was generated by extracting a single voltage sensor domain (S1–S4, residues P161–S307) from the chimera x-ray structure (PDB 2R9R) (13). A 70 × 70 Å POPC bilayer patch oriented in the *x*,*y* plane was built using the membrane package of VMD (37) and converted to a hexagonal box in GROMACS. The voltage sensor was inserted into this membrane using orientation information provided by the OPM database (38). Overlapping lipids and waters were deleted, such that 49 lipids per monolayer remained. The protein was modeled with the AMBER03 force field (39), POPC interactions were described with the Berger force-field parameters (40), and water was used as the TIP3P model (41). After energy minimization and equilibration of the bilayer, the system was solvated with 6995 waters and neutralized with chloride counterions.

All simulations were carried out with a development version of the GROMACS (42) package using 2-fs time steps. Bond lengths were constrained with the LINCS algorithm (43) and SETTLE (44) was used for water molecules. Electrostatic interactions were evaluated using particle-mesh Ewald summation every step. A 1.2-nm cutoff was used both for electrostatics and van der Waals interactions, with neighborlists updated every 10 steps. Simulations were performed at 300 K by using a Bussi thermostat (45). Semiisotropic pressure coupling was used during equilibration, but then turned off to avoid system fluctuations. The final configuration comprises a bit over 28,000 atoms, and was equilibrated for another 50 ns before production runs were performed.

Steered molecular simulations of S4

The pathway and work required for translation of S4 in both conformations was calculated from SMD. The reaction coordinate should be chosen such as to minimize the effect of the biasing force on the sampling. Because the strongest interactions here are believed to be between the S4 arginine side chains and other residues, the biasing force was set to act on them. To achieve a single reaction coordinate, we used the center-of-mass of

the side chains of the arginines. Another alternative could have been a charge-weighted center, which would have caused a <1 Å shift. To translate the helix, a harmonic potential was applied between the center-of-mass of the R0–R6 charged side chains and the center-of-mass of the helices S1–S3:

$$V_{\mathrm{SMD}} = \frac{k}{2}[(\mathrm{COM}_{\mathrm{S4}} - \mathrm{COM}_{\mathrm{S1-S3}})\cdot \mathbf{a}_H - d(t)]^2. \quad (1)$$

Effectively, this means the SMD force is applied to an internal distance between S4 and S1–S3. Due to the shape of the water cavities around S4 and the related electrostatic field focusing (36), the SMD potential was applied along the local S4 helix axis $\mathbf{a}_H$ defined from residues 287 to 307 in S4, which makes angle of 12° with the membrane normal. The charged side chains of R0–R6 (on which the steering force acts) lie along the same axis. This has a <2% effect on the downward force, but avoids pulling S4 away from the rest of the protein. The force constant k was 10,000 kJ/mol/nm^2 and the reference distance $d(t)$ increased linearly with a speed of 6.1 Å/μs. Additional simulations were also performed with a higher speed of 24.4 Å/μs.

Not compensating for torque would lead to a large rotation of the entire protein, as this is energetically less costly than the transition barrier. To counteract this, rotation of the center-of-mass of helices S1–S3 was removed at every step. By only applying it to the reaction group, we avoid influencing the work profiles for S4. The average net motion of S1–S3 relative to the bilayer center-of-mass was -0.2 ± 0.6 Å and 0.1 ± 0.8 Å for the α- and 3_{10}-helix runs, respectively. The work is determined by integrating the SMD force over the displacement of the reference distance d. In the limit of slow simulations, it will converge to the free energy along the reaction coordinate. To reduce distortion and lock the secondary structures, Cα distance restraints of 1000 kJ/mol/nm^2 to the next turn residue were applied in S4. To increase the chance of finding a low work path and obtain standard errors based on sampling of different trajectories, three separate full microsecond simulations with different initial velocities were performed for each S4 conformation, leading to an aggregated simulation time of almost 8 μs. By using the Jarzynski relation (46), we estimate the final potential of mean force as the Boltzmann-weighted average of the three work samples, and error bars from their standard deviation. Due to the Jarzynski relation the standard error is asymmetric, i.e., the free energy could be significantly lower, but only ~k_BT higher. This is further strengthened in that the 3_{10}-helix transition is only roughly one standard error above $\Delta G = 0$ after the R4 transition. The resulting work profile mainly shows the effect of α-versus 3_{10}-helix in the Q1–R3 region of S4, because the R3–R6 region is already a 3_{10}-helix structure in the x-ray structure.

RESULTS

S4 3_{10}-helix facilitates downward motion compared to α-helix

Although it was not possible to pull slowly enough to derive statistically accurate work profiles for an entire downward transition for Q1–R4, results from initial simulations taking 128–512 ns for the entire motion indicate that the mechanism for each arginine side chain passing the hydrophobic zone appears to be superficially similar, which agrees well with the repeating arginine sequence pattern (see Fig. S1 in the Supporting Material). For this reason, we decided to focus on the very initial stage where R4 passes the hydrophobic zone, and extend this part to microsecond simulations. Three such simulations were performed for each of the 3_{10}- and α-helix conformations of the S4 segment (start/end conformations shown in Fig. S2), and the SMD force was integrated to obtain the average work and standard errors from Jarzynski weighting (see Methods).

Plotting the work against the pull reference position (Fig. 1 *C*) reveals an increase in slope roughly at the same time as the arginine enters the hydrophobic zone. Because this causes the virtual pull spring to extend, we also separately plot the actual S4 segment backbone displacement as a function of the reference position, and Fig. S3 shows it as a function of the S4 backbone displacement.

The actual barrier is a collective effect; for a charged side chain to move across the hydrophobic zone the entire S4 segment has to move with it, and this appears to require rearrangement of the salt bridges both for the α- and 3_{10}-helix structures. However, the barrier is almost a factor-two lower for 3_{10}-helix (~70 kJ/mol) compared to α-helix (~130 kJ/mol). After this peak, the total work for the all-3_{10}-helix decreases to ~20 kJ/mol again, which supports that the SMD simulation is slow enough for the main effect to be free energy differences rather than friction. One important reason for this difference appears to be that the 3_{10} conformation facilitates contacts between E183 and R2, because the latter side chain is rotated more toward the direction of the glutamates. When R2 interacts with E183, R3 starts competing with R4 for salt bridges with E226. In contrast, when the upper part of S4 is α-helix, R2 primarily interacts with water and lipids, R3 only with E183, and R4 with E226. Forcing S4 down requires the segment to rotate and transiently break these interactions, rather than the cascading swaps possible for the 3_{10} conformation (Fig. S4).

The motion of charged side chains across the hydrophobic zone appears to be coupled to conformational changes of F233. For each arginine passing, this phenyl ring flips aside-and-back to create an efficient hydrophobic lock (Fig. 3). The flipping is very pronounced and local for the 3_{10}-helix, whereas the α-helix rather distorts the entire hydrophobic zone. Because these interactions are local, F233 by itself cannot explain the difference between α- and 3_{10}-helix (it seems to be caused by the salt bridges above), but it might be central to accomplish

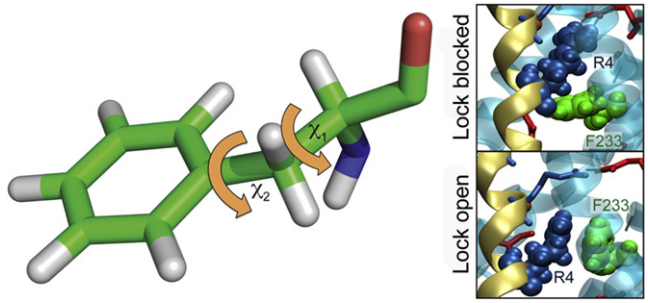

FIGURE 3 F233 is a structural obstruction for S4 arginines. The phenyl ring acts as a physical obstruction for arginines in the hydrophobic zone. For each arginine crossing this zone, the ring rotates away to open a passage in the hydrophobic zone, followed by a flip of the arginine side chain across the lock, and finally the ring rotates back to the original state. Interestingly, the rotation is upwards, which could indicate different kinetics for activation versus relaxation.

well-defined separate metastable states. This observed mechanism agrees well with recent mutation studies that show the importance of the ring structure to achieve a lock (47). Directly after passing the hydrophobic zone, the R4 side chain of the α-helix forms hydrogen bonds with D259, while it is stabilized by both E236 and D259 in the 3_{10}-helix, due to the side-chain orientation. Based on the shorter simulations, the subsequent arginine side chains (R3 and R2) likely cross the barrier in at least a qualitatively similar way.

Although this can be interpreted as support for a transition to increased 3_{10}-helix contents, possibly when moving from an open-inactivated (AL) to an open-active (A) state, it is important to remember that it does not take the cost of 3_{10}-helix formation into account. As covered in depth in the Discussion, this could cost ~2.4 kJ/mol per residue in a protein, but because spontaneous 3_{10}-helix growth has been observed in simulations with applied potential (22,28,29) it is possible that the total 3_{10}-contents in S4 is roughly the same in the up- and down-states, which could largely cancel the cost.

With a membrane potential of ~130 mV, the energy for translating a single charged side chain across the membrane is 12.5 kJ/mol. Because the field is focused inside the VSD even a small downward move of S4 can effectively subject a side chain to 80–100% of the full potential drop (22). Although the α- and 3_{10}-helix systems have very different initial conformations, it is interesting to consider the displacement charge during the downward motion, similar to Khalili-Araghi et al. (22). As shown in Fig. S5, for the α-helix there is a continuous change which involves both R4 passing the hydrophobic zone and breaking of other salt bridges, whereas the 3_{10}-helix system in contrast exhibits a virtually constant displacement charge until R4 passes the hydrophobic zone and contributes 0.83e, close to the value 0.81e calculated for the overall R4 contribution between open/closed states by Khalili-Araghi et al. (22). Our work difference when the first residue has passed the barrier for S4 in 3_{10}-helix conformation is 20 kJ/mol, which is within a factor-two of explaining the relative stability of the different states with the applied potential. The remaining difference could be due to friction in the simulation, but it is also possible that the model here does not capture all effects of a real potential caused by ion concentration differences. The fact that the VSD rarely seems to adopt intermediate states in vitro also suggests that the initial barrier dominates the process, with a larger fraction of the total gating charge (48). In contrast to this, stabilizing the α-helix after the barrier would require an energy several times higher than what can be explained from physiological potentials.

A 3_{10}-helix perturbs the VSD structure less than an α-helix

The distortion of the protein can be assessed by calculating the root mean-square deviation (RMSD) of segments S1–S3

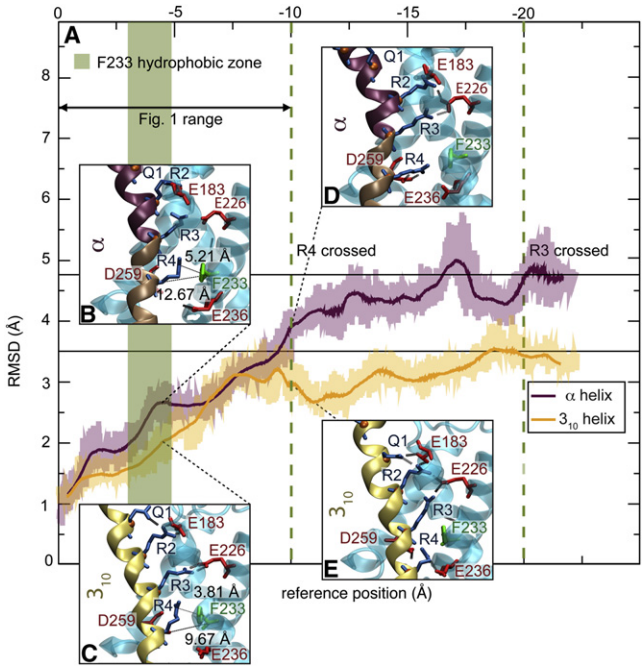

FIGURE 4 S4 translation as 3_{10}-helix perturbs the VSD less than α-helix. (*A*) Cα-RMSD for segments S1–S3 during 1 μs of pulling of S4 across the first barrier as α- (*purple*) versus 3_{10}-helix (*yellow*). RMSD was calculated relative to the initial conformation after a least-squares fitting of S1–S3, and shown with a 1-ns running average. The main difference occurs when R4 crosses the hydrophobic zone, which induces more distortion when S4 is in α-helix conformation. (*Insets*) Conformations before (*B* and *C*) and after (*D* and *E*) crossing the barrier, where the α-helix loses contact with E236.

as a function of the S4 pull reference position. As evident from Fig. 4, the 3_{10}-helix conformation of S4 results in significantly lower perturbation of the rest of the VSD compared to an α-helix. The reason for this appears to be that the side-chain conformations of the 3_{10}-helix only requires F233's ring to flip aside for each arginine whereas S4 translates down, and there is a cascade of salt-bridge swapping with higher arginines. In contrast, the α-helix conformation requires a rotation of S4 for each arginine that in turn will cause clashes with other parts of the VSD, and transiently broken salt bridges. In addition, the smaller radius of the 3_{10}-helix (compare panels *C* and *D* of Fig. 2) and the fact that all side chains line up in a triangular geometry seems to be more advantageous in the densely packed environment of the S4 translation pathway. This is supported by the RMSD behavior, where there is a first separation when R4 approaches the hydrophobic zone (Fig. 2, *C* and *D*). The distance between R4 and S1–S3 increases at this stage, with a clearly larger displacement for the α-helix compared to 3_{10}. When R4 has entirely passed the barrier, ~5.5 Å of S4 helix displacement (corresponding to a spring displacement of 8 Å), the difference between the structures, increases further. Whereas the 3_{10}-helix tends to converge at ~3.5 Å RMSD, the α-helix continues up to 4.5–5Å RMSD. One reason for this is that

R4 in the 3_{10}-helix shares hydrogen bonds with both E236 and D259 due to the induced rotation, whereas the same residue in the α-helix only interacts with D259.

The final polar glutamine (Q1) behaves roughly the same for both S4 conformations; due to the presence of both hydrogen bond donors and acceptors in this side chain, it will interact both with the glutamates (e.g., E183, Fig. 4 *E*) as well as the next arginine (R2) in the S4 helix. None of this rules out the S4 α-helix alternative, but it is clear that it requires larger conformational changes in the rest of the VSD, which is a likely contributing factor to the larger work required.

Hydrogen bond rearrangement is facilitated with 3_{10}-helix

Part of the conformation differences can be explained from differences in salt-bridge formation patterns. Before crossing the hydrophobic zone, the arginine side chains R4, R3, and R2 interact first with E183 and then E226. For both of these, there appears to be a common pattern for how the arginines do a hand-over of the hydrogen bonds. The arginine side chains can form hydrogen bonds with either N_ε or the two N_η as donors, and at equilibrium it is mainly the N_η that interact with the protein and lipids. As the side chains are forced down (mimicking an applied potential), the N_ε donor forms a new hydrogen bond with a glutamate (first E183, later E226), after which the arginine side chain rotates around its own axis and the main N_η hydrogen bonds move to the glutamate (Fig. S6). The process is virtually identical for the hand-over from lipids to E183 as for the hand-over E183 to E226. Interestingly, the number of hydrogen bonds before the barrier is roughly the same for S4 in both conformations, but the α-helix makes more hydrogen bonds to lipids that need to be broken before a downward motion is possible.

A similar pattern is observed after crossing the barrier, where the α-helix forms several hydrogen bonds with lipids (possibly related to the structural distortion). The 3_{10}-helix both maintains its existing hydrogen bonds longer and rapidly forms new ones with the acidic residues E236 and D259 when R4 passes the hydrophobic zone (Fig. S7). Compared to the tighter 3_{10} structure, this loss of hydrogen bonds, and resulting looser VSD structure, appears to be one reason for the higher work required for the α-helix downward motion.

Glutamates induce rotation, and might drive 3_{10} transition

To maintain hydrogen bonds with E183 and E226 as discussed above, the charged side chains in S4 are forced to rotate above F233 because the acidic residues are arranged in a circlelike geometry leading to the cavity (Fig. S8). This rotation does not continue below it due to the geometry of the hydrogen bond acceptors. This gives rise to a cumulative effect where the higher-located side chains (Q1, R2) rotate significantly (~100°). Below the hydrophobic zone, where the helix is already in 3_{10} conformation, K5/R4 largely maintain their side-chain direction (Fig. S8). R3 rotates slightly up to the point where it is passing F233, roughly to the same relative orientation as R4 was previously. This difference in orientation will lead to a tightening of the helix, which is likely to stabilize a 3_{10} conformation over α-helix as S4 translates down, which agrees well with observations of spontaneous 3_{10} formation in previous simulations (22,28,29). Although the backbone secondary structure restraints prevent this from happening in the nonequilibrium simulations, removing the restraints after R4 has crossed the barrier might lead to spontaneous extension of the 3_{10}-helix part. In contrast, when S4 is entirely in 3_{10} conformation, there is just a slight initial rotation of the side chains to let them interact with the acidic residues, and hydrogen bonds are predominantly formed with the $N_{\eta1}$+$N_{\eta2}$ donors.

Additional residues compete for hydrogen bonds with the glutamates. R3/R4 both interact with E226 (Fig. S5 *A*) and when R4 starts crossing the barrier it loses the hydrogen bond to E226 (*green area*, Fig. S5 *B*). Simultaneously, both R3 and R2 reorient and swap their N_ε hydrogen bonds with E226/E183 to have $N_{\eta1}$+$N_{\eta2}$ as new donors (Fig. S5). Throughout the process, there appear to be two typical conformations: metastable states where each acceptor glutamate has a single donor arginine, and transition states where two arginines interact with one glutamine (or vice versa).

Spontaneous α-to-3_{10} transition after barrier crossing

Based on the observed side-chain rotations, it is an obvious control to see what happens to an unrestrained helix after the barrier. Starting from an α-helix conformation where R4 has just crossed the hydrophobic zone and the work is decreasing, the system was run for 100 ns without any backbone restraints. Within 10 ns, the 3_{10}-helix is extended by one turn between R3 and R2, and remains stable for the 100-ns simulation. Exactly the same behavior is observed when the process is repeated for a snapshot when R3 has just crossed the barrier—in this case the 3_{10}-helix is extended from R2 to R1, and again stable for 100 ns (Fig. 5).

It is striking that the 3_{10}-helix in the x-ray structure extends to exactly this position between E183 and E226, which in the open state occurs between R4 and R3 (R4 interacting with E226 and R3 with E183). This suggests a possible gating model from the AL state where S4 has to make a turn-by-turn stepwise transition to 3_{10}-helix at the glutamates (Fig. 5 *D*), which could explain why this process is relatively slow. It is also possible for the segment below the barrier to convert back into α-helix. Simulations of closed state models do not entirely agree here (22,29),

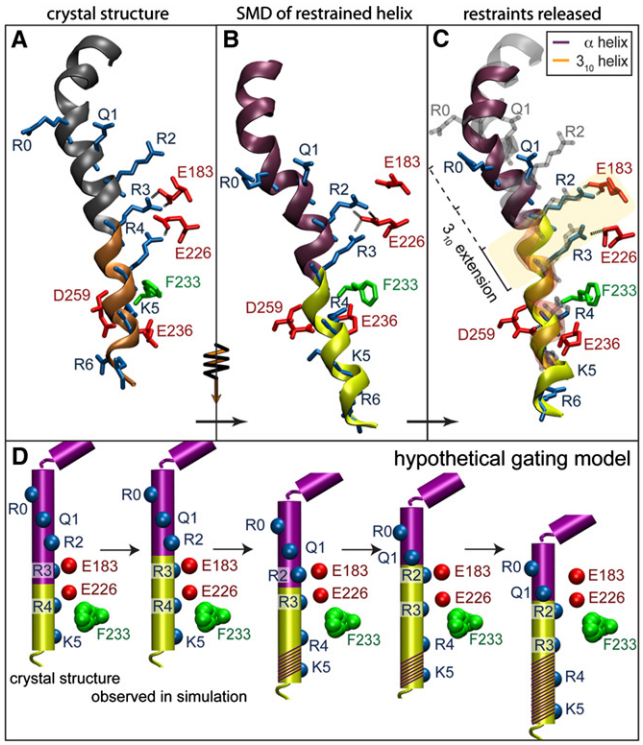

FIGURE 5 Spontaneous 3_{10} extension after forced barrier crossing. Pulling the crystal structure (*A*) with backbone restraints until R4 passes the hydrophobic zone (*B*) and then releasing restraints leads to formation of another 3_{10}-helix turn (*C*). R2 changes interaction partner from E226 to E183, which stretches/rotates the upper part of the helix and extends the 3_{10} region. The x-ray structure state is superimposed in shading. This confirms the large post-barrier free energy difference between α and 3_{10} predicted in Fig. 1. (*D*) Hypothetical model of gating when started from the AL state. Based on these and previous simulations (28), the applied polarization extends the 3_{10}-helix, which translates down with each arginine passing F233, and then the events are repeated. It is possible that S4 could go back to α-helix below the barrier (*dashed*), but because the 3_{10}-helix is seen in closed-state-model simulations (22,29) it is more likely that S4 is dominated by 3_{10}-helix in the normal open and relaxed states.

but we believe it would be advantageous for S4 to maintain 3_{10} structure all the way up to Q1 (and possibly R0). This could explain how the rapid normal activation/relaxation is different from slow inactivation, which might then be caused by the relaxation to α-helix in the upper part.

DISCUSSION

The potential cost of converting the upper part of S4 from α-helix into 3_{10} conformation is obviously a critical question. Unfortunately it is not yet possible to accurately calculate this inside the VSD structure, as the standard errors are much larger than the difference. There are also some arguments why this might not be a net cost.

First, previous simulations indicate S4 exhibits spontaneous 3_{10}-helix growth with applied potential or in the down state (without forcing any transition) (22,28,29). Second, even if there is a cost associated with this S4 transition, the model above suggests it would only be incurred when starting from the AL state—in the normal activation/relaxation cycle the helix could maintain its secondary structure to reduce this cost. Regardless of this, it is interesting to estimate the free energy difference.

Smythe et al. (49) calculated the cost of converting an entire decapeptide from α- to 3_{10}-helix in a proteinlike environment to roughly 24 kJ/mol, or 2.4 kJ/mol per residue (and the gas phase difference is another factor-two lower). Even if the entire upper half of S4 has to convert to 3_{10}, the cost is lower than the work difference we observe for the full S4 transition (Fig. 1 *C*). Thus, even if the 3_{10}-helix part did not grow spontaneously after applying polarization, it would be advantageous to make the conversion before S4 translation, rather than remaining as an α-helix. Interestingly, Smythe et al. (49) actually suggest already in their 1995 article that the low cost could make α- to 3_{10}-helix conversion important for some biological processes. The barrier for the backward transition is very low from the same studies (below 0.1 kJ/mol per residue), which suggests S4 could readily go back to α-helix. Because we do not observe this for residues that have crossed the barrier we believe it is a further indication that S4 might indeed stay as 3_{10}-helix in the relaxed and open-active states, but makes a transition to α-helix in the open-inactive state as it is reflected in the x-ray structure. This could potentially remove the otherwise hidden α- to 3_{10}-helix conversion cost entirely from the normal transition barrier, but further studies are required to confirm this. If the S4 segment stays largely as 3_{10}-helix during normal opening/closing, the conversion cost would only be incurred during the much slower open-active to open-inactive transition. Interestingly, this might also provide an explanation for the difference between normal activation and relaxation versus the transition to/from the inactive state.

It is a highly interesting question to what extent S4 might go back from 3_{10}- to α-helix after passing the barrier. Schow et al. (29) have recently derived a new higher-resolution down-state model of the related KvAP voltage sensor based on biotin-avidin accessibility and salt-bridge data, where they see S4 adopting α-helical conformation from downstream of R1–R4 in the relaxed state, i.e., the C-terminal end. Independently, Khalili-Araghi et al. (22) performed microsecond-scale refinement of the earlier Pathak model (20) and also observe spontaneous 3_{10} conversion for 10 residues in the extracellular half of S4.

A more realistic model for the actual gating could thus have the 3_{10} region moving roughly two turns along S4, and the residues facing the hydrophobic barrier would always be in 3_{10} conformation, which would work equally well thermodynamically in the sense that it avoids any net conversion cost for the entire S4 segment. Both Khalili-Araghi et al. (22) and Schow et al. (29) also point out the role of salt bridges and the intracellular aqueous crevice opening for stabilizing 3_{10} structure.

It is not obvious to explain how the S4 transition to the inactive state is different from normal relaxation-activation if the secondary structure always changes (in contrast to staying as 3_{10}-helix), but it is possible that the process could be different in different regions of S4. In this respect, the all-3_{10}-helix used as a simplified model in this work is obviously an extreme case because it is rare to find 3_{10}-stretches above 12 residues in proteins (50), but we cannot a priori calculate which residues would be most favorable to have in 3_{10}-helix. However, the secondary structure conformation at the terminal parts of the helix is not likely to affect the transition barrier significantly, as those parts are largely in the aqueous cavities rather than tightly packed in the protein interior. If anything, if it is clearly advantageous (in terms of free energy) for some parts of S4 to remain α-helix, it would simply reinforce the work difference reported here.

An important point is that even if these simulations sample multiple pathway trajectories, they are merely samples and obviously not the optimal minimum free energy pathway. Other pathways could provide even lower free energy, and playing the Devil's advocate, one could ask whether all those trajectories merely represent improbable pathways. However, there are also lower bounds on the expected free energy barrier that are useful to consider here. After the arginine has passed the hydrophobic barrier, the estimated free energy for the 3_{10}-helix goes down to at least ~20 kJ/mol (it is in fact still decreasing when the α-helix levels out).

In comparison, the free energy difference for a single charge moving across a 130 mV potential change should be ~12 kJ/mol, which is within the standard error bars. In other words, the 3_{10}-helix trajectories represent possible pathways that are compatible with the experimental results and within ~10 kJ/mol of a real pathway, because gating requires ~100 mV to occur. Together with spontaneous 3_{10}-helix formation, these pathways at least cannot be extremely improbable. In contrast, none of the α-helix pathways even come close to be compatible with a 10–20 kJ/mol barrier. Further, the rapid spontaneous 3_{10}-helix conversion after the barrier when the structure restraints are removed from the α-helix both indicates they sample neighboring regions of phase space, and that the 3_{10} helix indeed has lower free energy in this conformation. The observed profile for the 3_{10}-helix is compatible with a model where the membrane polarization changes the resting state to be more stable than the activated one, although there is still a significant—but surmountable—barrier between them.

Although the actual free energy barrier is a complex collective process related to S4 rotation and salt bridges, F233 appears to have a prominent role in the hydrophobic lock zone. It is also the only residue in this zone that exhibits direct dynamics correlated with the S4 and arginine side-chain translation. In contrast, I230 is almost equally bulky and located just one turn above F233, and the I230H mutation has been shown to generate a proton pore in the closed state (51). However, although this residue clearly helps to form the lock and interacts with F233, it does not appear to move much itself. The exact details of the barrier that prevents S4 from moving back to the resting state are still unknown, but mutations on residues such as F233, I230, and I177 are important future projects that might be possible to address with equilibrium methods by starting from the steered pathways for the wild-type protein.

In summary, we believe there is increasingly strong qualitative as well as quantitative evidence from simulations that an altered 3_{10}-helix segment in S4 is a core component in the transition and that it significantly reduces the work required to pass the barrier. This could help reconcile differences between the conceptual models, and potentially provides a very natural explanation for the separate much slower transition to the AL state.

SUPPORTING MATERIAL

Detailed methods description, supporting figures, and movies of S4 transition are available at http://www.biophysj.org/biophysj/supplemental/S0006-3495(11)00191-3.

The authors thank F. Elinder, S. Pronk, and J. Trudell for many helpful discussions. Supercomputing resources were provided by the Swedish National Infrastructure for Computing.

This work was supported by grants to E.L. from the European Research Council (No. 209825), the Swedish Foundation for Strategic Research, and the Swedish Research Council.

REFERENCES

1. Tombola, F., M. M. Pathak, and E. Y. Isacoff. 2006. How does voltage open an ion channel? *Annu. Rev. Cell Dev. Biol.* 22:23–52.
2. Aggarwal, S. K., and R. MacKinnon. 1996. Contribution of the S4 segment to gating charge in the *Shaker* K^+ channel. *Neuron.* 16:1169–1177.
3. Seoh, S. A., D. Sigg, …, F. Bezanilla. 1996. Voltage-sensing residues in the S2 and S4 segments of the *Shaker* K^+ channel. *Neuron.* 16:1159–1167.
4. Horn, R. 1998. Explorations of voltage-dependent conformational changes using cysteine scanning. *Methods Enzymol.* 293:145–155.
5. Cha, A., G. E. Snyder, …, F. Bezanilla. 1999. Atomic scale movement of the voltage-sensing region in a potassium channel measured via spectroscopy. *Nature.* 402:809–813.
6. Glauner, K. S., L. M. Mannuzzu, …, E. Y. Isacoff. 1999. Spectroscopic mapping of voltage sensor movement in the *Shaker* potassium channel. *Nature.* 402:813–817.
7. Murata, Y., H. Iwasaki, …, Y. Okamura. 2005. Phosphoinositide phosphatase activity coupled to an intrinsic voltage sensor. *Nature.* 435:1239–1243.
8. Sasaki, M., M. Takagi, and Y. Okamura. 2006. A voltage sensor-domain protein is a voltage-gated proton channel. *Science.* 312:589–592.
9. Okamura, Y. 2007. Biodiversity of voltage sensor domain proteins. *Pflugers Arch.* 454:361–371.
10. Kohout, S. C., M. H. Ulbrich, …, E. Y. Isacoff. 2008. Subunit organization and functional transitions in Ci-VSP. *Nat. Struct. Mol. Biol.* 15:106–108.

11. Freites, J. A., D. J. Tobias, and S. H. White. 2006. A voltage-sensor water pore. *Biophys. J.* 91:L90–L92.
12. Sands, Z. A., and M. S. Sansom. 2007. How does a voltage sensor interact with a lipid bilayer? Simulations of a potassium channel domain. *Structure.* 15:235–244.
13. Long, S. B., X. Tao, …, R. MacKinnon. 2007. Atomic structure of a voltage-dependent K^+ channel in a lipid membrane-like environment. *Nature.* 450:376–382.
14. Yang, N., and R. Horn. 1995. Evidence for voltage-dependent S4 movement in sodium channels. *Neuron.* 15:213–218.
15. Bezanilla, F. 2002. Voltage sensor movements. *J. Gen. Physiol.* 120:465–473.
16. Catterall, W. A. 1986. Molecular properties of voltage-sensitive sodium channels. *Annu. Rev. Biochem.* 55:953–985.
17. Ahern, C. A., and R. Horn. 2004. Stirring up controversy with a voltage sensor paddle. *Trends Neurosci.* 27:303–307.
18. Guy, H. R., and P. Seetharamulu. 1986. Molecular model of the action potential sodium channel. *Proc. Natl. Acad. Sci. USA.* 83:508–512.
19. Jiang, Y., V. Ruta, …, R. MacKinnon. 2003. The principle of gating charge movement in a voltage-dependent K^+ channel. *Nature.* 423:42–48.
20. Pathak, M. M., V. Yarov-Yarovoy, …, E. Y. Isacoff. 2007. Closing in on the resting state of the *Shaker* K^+ channel. *Neuron.* 56:124–140.
21. Yarov-Yarovoy, V., D. Baker, and W. A. Catterall. 2006. Voltage sensor conformations in the open and closed states in ROSETTA structural models of K^+ channels. *Proc. Natl. Acad. Sci. USA.* 103:7292–7297.
22. Khalili-Araghi, F., V. Jogini, …, K. Schulten. 2010. Calculation of the gating charge for the Kv1.2 voltage-activated potassium channel. *Biophys. J.* 98:2189–2198.
23. Noda, M., S. Shimizu, …, S. Numa. 1984. Primary structure of *Electrophorus electricus* sodium channel deduced from cDNA sequence. *Nature.* 312:121–127.
24. Kosower, E. M. 1985. A structural and dynamic molecular model for the sodium channel of *Electrophorus electricus*. *FEBS Lett.* 182:234–242.
25. Clayton, G. M., S. Altieri, …, J. H. Morais-Cabral. 2008. Structure of the transmembrane regions of a bacterial cyclic nucleotide-regulated channel. *Proc. Natl. Acad. Sci. USA.* 105:1511–1515.
26. Shafrir, Y., S. R. Durell, and H. R. Guy. 2008. Models of voltage-dependent conformational changes in NaChBac channels. *Biophys. J.* 95:3663–3676.
27. Villalba-Galea, C. A., W. Sandtner, …, F. Bezanilla. 2008. S4-based voltage sensors have three major conformations. *Proc. Natl. Acad. Sci. USA.* 105:17600–17607.
28. Bjelkmar, P., P. S. Niemelä, …, E. Lindahl. 2009. Conformational changes and slow dynamics through microsecond polarized atomistic molecular simulation of an integral Kv1.2 ion channel. *PLOS Comput. Biol.* 5:e1000289.
29. Schow, E. V., J. A. Freites, …, D. J. Tobias. 2010. Down-state model of the voltage-sensing domain of a potassium channel. *Biophys. J.* 98:2857–2866.
30. Catterall, W. A. 1986. Voltage-dependent gating of sodium channels: correlating structure and function. *Trends Neurosci.* 9:7–10.
31. Papazian, D. M., X. M. Shao, …, D. H. Wainstock. 1995. Electrostatic interactions of S4 voltage sensor in *Shaker* K^+ channel. *Neuron.* 14:1293–1301.
32. Karpen, M. E., P. L. de Haseth, and K. E. Neet. 1992. Differences in the amino acid distributions of 3_{10}-helices and α-helices. *Protein Sci.* 1:1333–1342.
33. Tobias, D. J., and C. L. Brooks, 3rd. 1991. Thermodynamics and mechanism of α-helix initiation in alanine and valine peptides. *Biochemistry.* 30:6059–6070.
34. Swartz, K. J. 2008. Sensing voltage across lipid membranes. *Nature.* 456:891–897.
35. Islas, L. D., and F. J. Sigworth. 2001. Electrostatics and the gating pore of *Shaker* potassium channels. *J. Gen. Physiol.* 117:69–89.
36. Asamoah, O. K., J. P. Wuskell, …, F. Bezanilla. 2003. A fluorometric approach to local electric field measurements in a voltage-gated ion channel. *Neuron.* 37:85–97.
37. Humphrey, W., A. Dalke, and K. Schulten. 1996. VMD: visual molecular dynamics. *J. Mol. Graph.* 14, 33–38., 27–28.
38. Lomize, M. A., A. L. Lomize, …, H. I. Mosberg. 2006. OPM: orientations of proteins in membranes database. *Bioinformatics.* 22:623–625.
39. Duan, Y., C. Wu, …, P. Kollman. 2003. A point-charge force field for molecular mechanics simulations of proteins based on condensed-phase quantum mechanical calculations. *J. Comput. Chem.* 24:1999–2012.
40. Berger, O., O. Edholm, and F. Jähnig. 1997. Molecular dynamics simulations of a fluid bilayer of dipalmitoylphosphatidylcholine at full hydration, constant pressure, and constant temperature. *Biophys. J.* 72:2002–2013.
41. Jorgensen, W. L., J. Chandrasekhar, …, M. L. Klein. 1983. Comparison of simple potential functions for simulating liquid water. *J. Chem. Phys.* 79:926–935.
42. Hess, B., C. Kutzner, …, E. Lindahl. 2008. GROMACS 4.0: algorithms for highly efficient, load-balanced, and scalable molecular simulation. *J. Chem. Theory Comput.* 4:435–447.
43. Hess, B., H. Bekker, …, J. Fraaije. 1997. LINCS: a linear constraint solver for molecular simulations. *J. Comput. Chem.* 18:1463–1472.
44. Miyamoto, S., and P. A. Kollman. 1992. SETTLE: an analytical version of the SHAKE and RATTLE algorithm for rigid water models. *J. Comput. Chem.* 13:952–962.
45. Bussi, G., and M. Parrinello. 2007. Accurate sampling using Langevin dynamics. *Phys. Rev. E Stat. Nonlin. Soft Matter Phys.* 75:056707.
46. Jarzynski, C. 1997. Nonequilibrium equality for free energy differences. *Phys. Rev. Lett.* 78:2690–2693.
47. Tao, X., A. Lee, …, R. MacKinnon. 2010. A gating charge transfer center in voltage sensors. *Science.* 328:67–73.
48. Bezanilla, F. 2000. The voltage sensor in voltage-dependent ion channels. *Physiol. Rev.* 80:555–592.
49. Smythe, M. L., S. E. Huston, and G. R. Marshall. 1995. The molten helix: effects of solvation on the α-to-3_{10}-helical transition. *J. Am. Chem. Soc.* 117:5445–5452.
50. Pal, L., and G. Basu. 1999. Novel protein structural motifs containing two-turn and longer 3_{10}-helices. *Protein Eng.* 12:811–814.
51. Campos, F. V., B. Chanda, …, F. Bezanilla. 2007. Two atomic constraints unambiguously position the S4 segment relative to S1 and S2 segments in the closed state of *Shaker* K channel. *Proc. Natl. Acad. Sci. USA.* 104:7904–7909.